Adsorption of copper from water using TiO$_2$-modified activated carbon derived from orange peels and date seeds: Response surface methodology optimization

Roya Sadat Neisan [a], Noori M.Cata Saady [a,*], Carlos Bazan [b], Sohrab Zendehboudi [c], Talib M. Albayati [d]

[a] Department of Civil Engineering, Faculty of Engineering and Applied Science, Memorial University of Newfoundland, St. John's, NL, A1B 3X5, Canada
[b] Faculty of Business Administration, Memorial University of Newfoundland, St. John's, NL, A1B 3X5, Canada
[c] Department of Process Engineering, Memorial University of Newfoundland, St. John's, NL, A1B 3X5, Canada
[d] Department of Chemical Engineering, University of Technology - Iraq, 52 Alsinaa St., PO Box 35010, Baghdad, Iraq

ARTICLE INFO

ABSTRACT

This study evaluated the application and efficiency of modified activated carbon in the removal of copper (Cu) from synthetic aquatic samples. The surface of activated carbon derived from orange peel (AC-OP) and date seeds (AC-DS) have been modified by Titanium dioxide nanoparticles (TiO$_2$ NPs) (1:10 wt% mixing ratio) and used in a series of experiments designed by Response Surface Methodology (RSM) incorporating Central Composite Design (CCD). The Brunauer-Emmett-Teller (BET) test demonstrated that the modification has increased the surface area of AC-OP from 2.40 to 6.06 m^2 g^{-1} and AC-DS from 51.10 to 81.37 m^2 g^{-1}. Effects of pH (1–7), ion initial concentration (10–60 mg L^{-1}), adsorbent dose (0.5–8 g L^{-1}), and contact time (0.4–6 h) have been investigated. The results showed that the optimum conditions for TiO$_2$-modified AC-OP (OP–TiO$_2$) are pH 5, initial concentration of 24.6 mg L^{-1}, adsorbent dose of 4.9 g L^{-1}, and contact time of 3.6 h. The optimum conditions for TiO$_2$-modified AC-DS (DS-TiO$_2$) are pH 6.4, initial concentration of 21.2 mg L^{-1}, adsorbent dose of 5 g L^{-1}, and contact time of 3.0 h. The modified quadratic models represented the results well with regression coefficients of 0.91 and 0.99 for OP-TiO$_2$ and DS-TiO$_2$, respectively. The maximum Cu removal for OP-TiO$_2$ and DS-TiO$_2$ were 99.90 % and 97.40 %, and the maximum adsorption capacity was found to be 13.34 and 13.96 mg g^{-1}, respectively. Kinetic data have been fitted to pseudo first-order, pseudo second-order, intra-particle diffusion, and Elovich models. The pseudo second-order showed a better fit to the experimental data (R^2 > 98 %). This study demonstrates the successful development of modified activated carbon derived from orange peels and date seeds, modified by TiO$_2$ nanoparticles, for efficient adsorption of copper ions from water. The findings contribute to understanding the adsorption mechanism and provide valuable insights for designing environmentally friendly adsorbents.

* Corresponding author.
  E-mail address: nsaady@mun.ca (N.M.Cata Saady).

1. Introduction

Pollution of water sources by heavy metals has increased globally as a result of rising industrial activity and improper water and wastewater treatment. Drinking water contamination is the main route exposing humans to heavy metals. Drinking water contaminated with heavy metals has been linked to several harmful consequences on human metabolism. The formation of reactive oxygen species, i.e., oxidative damage, is the main mechanism of adverse effects on people's health, leading to high rates of disease and fatalities worldwide [1,2].

Copper (Cu, molecular weight: 63.5 g mol^{-1} and oxidation state +1, +2) [2] is one of the most toxic metals which is irresponsibly released into the environment by various activities, such as metal processing, coal combustion, Copper photogravure, and tire manufacturing. The World Health Organization (WHO) has determined the maximum copper concentration in drinking water at 2 mg L^{-1} due to health risks caused by copper exposure. High Cu consumption may result in gastrointestinal issues, liver or kidney damage, nervous system disorders acute hemolytic anemia, capillary damage, and in severe cases, even death. Considering such toxic effects in human health and aquatic systems, Cu removal from drinking water sources and wastewater before its discharge is crucial [3,4].

Among the common heavy metal removal technologies such as coagulation–flocculation, ion exchange, and membrane technologies, the most popular one, absorption, is widely used because of abundant low-cost and renewable materials that can be converted to adsorbents, easy operation, low cost, removal and energy efficiency, and ability to remove various contaminants [3,5]. Various adsorbents have been used to remove Cu from water and wastewater, including polymeric fibers [6], nanomaterials [7], modified natural materials [8], agricultural waste [9], industrial waste [10], and carbon-based materials [11]. However, activated carbon has long been the preferred adsorbent in heavy metal removal due to its excellent adsorption capacity, rate, porosity, and high surface area [12]. The need for developing more affordable and effective adsorbents from renewable sources has been prompted by the high cost of commercial activated carbon [13]. Biochar is a type of carbon-rich substance made by pyrolyzing biomass at high temperatures in an inert environment. However, it has generally poor adsorption capability. Surface chemical modification could solve this problem because it enhances the functional groups, active sites, and surface structure of biochar [5]. Recently, agricultural waste such as orange peels and date seeds have been used to remove heavy metals from aquatic sources. Table 1 summarizes the removal efficiency and adsorbent capacity of recently developed adsorbents from orange peels and date seeds.

Despite the extensive research on the adsorption of heavy metals from water using various adsorbents, limited attention has been given to removing copper from water using TiO$_2$-modified activated carbon derived from agricultural waste materials such as orange peels and date seeds. In this study, the primary objective is to investigate copper adsorption from water using modified activated carbon derived from orange peels and date seeds. By modifying the activated carbon through the incorporation of TiO$_2$ nanoparticles, we aim to enhance its adsorption capacity and efficiency for copper removal. Recently, there has been a growing interest in utilizing TiO$_2$ for various applications, including environmental purification and adsorption processes [24]. The TiO$_2$ excellent physical and chemical properties, including its large surface area, and abundant active sites make it particularly attractive for removing heavy metals and organic pollutants [24,25]. However, the practical application of TiO$_2$ nanoparticles faces challenges such as agglomeration, reduced surface area, and difficulties in recovery [26]. To overcome these limitations, combining nanostructured materials, such as TiO$_2$, with carbon-based materials has been shown to enhance the overall efficiency of adsorption processes in water [25]. The

Table 1
Summary of adsorptive removal of heavy metals by relevant adsorbents.

Adsorbent	Adsorbate	IC (mg L^{-1})	Adsorbent dose (g L^{-1})	pH	Contact time (min)	Other Info	RE (%) or/and AC (mg g^{-1})	Ref.
Modified orange peel	Cd(II) Ni(II)	50	30 25	6	180	25 °C 200 rpm	91.0 % 93.4 %	[14]
Fe(II)/Fe(III) modified orange peel	As(V)	40	200	6	300	Fe/biomass ratio is 10 wt %, 300 rpm	81.3 mg g^{-1}	[15]
Chitosan/orange peel hydrogel composite	Cr(VI) Cu(II)	100	40	4 5	360	200 rpm room temperature	80.4 % 82.5 %	[16]
Orange peels modified with magnetic nanoparticles	As(III)	40	1	7	720	180 rpm	10.3 mg g^{-1} 98.5 %	[17]
Orange peel modified with mercaptoacetic acid (C$_2$ H$_2$ O$_2$ S)	As(V) Cu(II) Pb(II)	80	2	6	120	220 rpm	34.0 mg g^{-1} 50.0 mg g^{-1} 43.5 mg g^{-1}	[18]
Date seeds powder	Ni(II)	50	6	7	30	150 rpm 25 °C	90 %	[19]
Activated carbon from date seeds	Cr(VI)	50	2	2	60	30 °C	42.6 mg g^{-1}	[20]
Carbonized date seeds	Pb(II)	5	6	5	2	25 °C 120 rpm	88.5 %	[21]
Microwave-assisted modified date seed Husk	As (III)	25	10	4	45	250 rpm	85 % 1.3 mg g^{-1}	[22]
Date seeds biochar	Cd(II), Cr(III), Co (II), Cu(II), Pb(II), Mn(II)	2	2	NA	overnight	200 rpm	93.3 % 71.1 % 92.1 % 97.0 % 95.9 % 36.1 %	[23]

IC = initial concentration; RE = Removal efficiency; AC = Adsorption capacity.

significance of this research is in its potential contribution to addressing the pressing challenges associated with copper contamination in water. Understanding the factors influencing the adsorption process and optimizing the conditions for maximum copper removal are crucial aspects of this study. By exploring the effects of various process variables and employing response surface methodology (RSM) for optimization, we aim to achieve improved adsorption efficiency while minimizing resource consumption.

Emerging research has demonstrated the effectiveness of response surface methodology (RSM) as a potent statistical tool in optimizing process parameters [27–29]. The application of response surface methodology (RSM) entails an empirical modeling approach aimed at evaluating the correlation between process variables and corresponding outputs [27]. The utilization of RSM for optimizing the conditions offers notable advantages, such as time and chemical savings. Additionally, it contributes to a deeper comprehension of the factors influencing the performance of the adsorbent [30]. The optimization of process parameters was carried out using the RSM with the Central Composite Design (CCD) implemented through Design Expert software. The CCD includes axial star points in its design, enabling improved estimation of RSM curves. RSM-CCD provides more flexibility in exploring the response space and capturing the behavior at extreme cases, such as the corners or edges of the design space [31–34]. Although the BBD statistical method offers benefits in terms of process optimization by a smaller number of experiments and reduced operational costs [35], the CCD allows for more levels per factor, with five different levels for each factor, including points both within and outside the specified limits [31–34]. In addition to optimization studies, comprehensive kinetic studies have been conducted to examine the dynamic behavior of copper removal using the TiO_2-modified activated carbon derived from orange peels and date seeds. By investigating the adsorption kinetics, valuable insights were obtained regarding the rate of copper ion adsorption onto the adsorbent surface and the time required to achieve equilibrium. Adsorption kinetics were performed and compared to pseudo first-order and second-order kinetic models. Several physiochemical characterizations were used to study the modified activated carbon's surface and functional groups.

2. Materials and methods

The titanium dioxide Nano powder (TiO_2, anatase, 99.9 %, 18 nm) and copper (II) sulfate pentahydrate ($CuSO_4\ 5H_2O$) were purchased from US Research Nanomaterials (Texas, U.S) and Acros Organics (New Jersey, U.S), respectively. Carbon dioxide and nitrogen of 99.99 % purity were purchased from Praxair Canada Inc. The orange peels and dates were collected from local markets in St John's, NL. Cu(II) solution (60 mg L^{-1}) has been prepared by dissolving $CuSO_4\ 5H_2O$ in deionized water. The stock solution has been diluted to provide the required solution concentrations. Physical and chemical characteristics of materials are investigated through characterization studies in order to understand better the efficacy of the procedure used to create the adsorbents and the adsorption mechanisms. The surface morphology and the chemical elements of all adsorbents were studied using a Field emission detector Scanning Electron Microscope (SEM) coupled to an energy-dispersive X–ray spectroscopy (EDX) to perform particle elemental analysis (JSM-7100 F, JEOL Ltd, Japan). A Bruker Tensor 27 Fourier transform infrared spectrometer (FT-IR) working in the ZnSe ATR mode in the range of 4000–650 cm^{-1} at a spectral resolution of 4 cm^{-1} for 32 scans has been used to identify the functional surface groups. The elements in the materials and the structural composition have been characterized using an X–ray diffraction (XRD) with Cu source and scintillation detector (Ultima-IV, 40 kV/44 mA, Rigaku, Japan). A surface area analyzer (Tristar II 3020, Micromeritics, US) has been used for nitrogen adsorption–desorption at 77 K for measuring specific surface area.

2.1. Preparation of adsorbents

2.1.1. Activated carbon from orange peels and date seeds

Date seeds and orange peels have been converted to activated carbon using the following procedure. The biomass has been washed thoroughly with distilled water and oven-dried at 80 °C for 6 h. The dried biomass has been ground using a mortar and pestle followed by a grinder. Once ground, it was passed through a 506 μm sieve. The carbonization and activation experiments have been conducted in a tubular furnace reactor (Lindberg/Blue M, TF55035A-1, US). The carbonization temperature has been controlled at 500 °C for orange peels and seed dates powders. During the carbonation process, the reactor has been heated to the target temperature at 10 °C min^{-1} heating rate, under nitrogen gas (N_2), and the N_2 flow rate has been controlled at 100 mL min^{-1}. The samples have been kept at the target temperature for 2 h. After 2 h, the nitrogen gas valve has been closed and carbon dioxide (CO_2) gas has been connected. The sample has been kept under CO_2 gas for 1 h at 100 mL min^{-1}.

2.1.2. Modification of activated carbon by titanium dioxide nanoparticles

Titanium dioxide nanoparticles have been fabricated using ultrasonication methodology. For every 1.0 g of activated carbon from each material, 0.1 g of TiO_2 nanoparticles were added to a flask containing 50 mL of distilled water. Then, the flask has been

Table 2
The ranges and levels of independent parameters.

Parameter	Unit	−1	+1	-α	+α
A-pH		2.2	5.8	1.0	7.0
B-Initial concentration	mg L^{-1}	20.0	50.0	10.0	60.0
C-Adsorbent dose	g L^{-1}	2.0	6.4	0.5	8.0
D-Contact time	h	1.3	4.8	0.4	6.0

ultrasonicated for 30 min at room temperature. The resultant suspensions have been filtered and washed 4–5 times with distilled water. Finally, the resulting wet material has been oven-dried overnight at 65 °C.

2.2. Experimental design

The central composite design (CCD), a common experimental design of RSM, has been utilized to develop the relationship between the process factors and response which is the removal efficiency. In order to determine the optimum values of pH, metal ion concentration, biomass dosage, and contact time, the CCD created an experimental design matrix for four variables (Table 2). A second-order polynomial response surface model can be used to fit the experimental data (Eq. (1)):

$$R = \beta_0 + \sum_{i=1}^{4} \beta_i x_i + \sum_{i=1}^{4} \sum_{i>j} \beta_{ij} x_i x_j + \sum_{i=1}^{4} \beta_{ii} x_i^2 + \varepsilon \tag{1}$$

where R stands for the expected response (removal efficiency (%)), and β_0, β_i, β_{ii}, β_{ij}, and ε represent the offset, the linear effect, the squared effect, the interaction impact, and the residual term, respectively. The coded independent variables (pH, contact time, initial concentration, and adsorbent dose) are represented by x_i and x_j. A total number of 21 experiments have been designed by Design Expert software (version 12.0.8.0, Stat–Ease Inc., Minneapolis, MN, USA).

2.3. Adsorption experiments

Adsorption batch tests have been conducted based on the CCD design, and the impact of the adsorption factors on the removal of Cu (II) from aqueous solution has been investigated. Different concentrations of Cu solution have been prepared and a known amount of adsorbents were added to 50 mL Erlenmeyer flasks containing Cu solution at the desired pH. The pH of the metal solutions has been adjusted using 0.1 M and 1 M solution of hydrochloric acid (HCl) and sodium hydroxide (NaOH). The flasks have been then placed on an orbital shaker with a speed of 200 rpm for a given time. All experiments have been carried out at room temperature. The mixture has been filtered and analyzed using an inductively coupled plasma–optical emission spectrometer, ICP-OES (Optima 5300 DV, Perki-nElmer, US).

The adsorption efficiency or removal percentage of contaminants and the adsorption capacity of the adsorbents have been calculated using Eqs. (2) and (3), respectively.

$$\% \, Adsorption = \frac{C_0 - C_t}{C_0} \times 100 \tag{2}$$

$$q_t = (C_0 - C_t) V / m \tag{3}$$

where C_0 and C_t are initial and final (at time t) concentrations of the metal ions, respectively, q_t (mg g^{-1}) is the mass of adsorbate per mass of adsorbent at time t, V is the volume of the solution (L), and m is the mass of adsorbent (g) [36].

2.4. Kinetic studies

The adsorption mechanism of Cu(II) has been studied using four different kinetic models. The kinetic study has been conducted for the time span of 5–240 min under optimum conditions at room temperature.

Pseudo first-order model (Eq. (4)) describes the adsorption of adsorbate onto the surface of the adsorbent and follows the first-order mechanism.

$$log \, q_e - q_t = log \, q_e - \left(\frac{K_1}{2.303}\right) t \tag{4}$$

where q_e is the adsorption capacity at equilibrium (mg g^{-1}), k_1 is the adsorption rate constant (g mg^{-1} h^{-1}).

Based on pseudo second-order kinetics, the adsorption kinetics may be described by Eq. (5):

$$t / q_t = 1/q_e^2 k_2 + t/q_e \tag{5}$$

where k_2 is the reaction rate constant (g mg^{-1} h^{-1}), q_e is the amount of solute adsorbed at equilibrium (mg g^{-1}), and q_t is the amount of solute adsorbed at time t [37]. A straight line may be formed from a t/q_t vs. t plot and used to determine k_2 and q_e. The value of k_2 can be calculated from the interception and slope of the graph as $k_2 = (Slop)^2/Intercept$ and q_e is determined by 1/slope [38].

In addition to pseudo first-order and pseudo second-order models, the intra-particle diffusion, and Elovich kinetic models were also applied to study the adsorption mechanism of Cu(II). The intraparticle diffusion model assumes that the adsorption process occurs through the diffusion of adsorbate molecules within the adsorbent particles. This model is represented by Eq. (6):

$$q_t = k_i t^{0.5} + C \tag{6}$$

where k_i is the intraparticle diffusion rate constant (mg g^{-1} h$^{-0.5}$), and C is the intercept which reflects thickness of the boundary

layer. The plot of q_t against $t^{0.5}$ can provide insights into the involvement of intraparticle diffusion in the adsorption process.

The Elovich kinetic model suggests that the adsorption process involves chemisorption and the formation of a monolayer on the adsorbent surface. The equation for the Elovich model is Eq. (7):

$$q_t = \left(\frac{1}{\beta}\right) \ln\left(\alpha\beta\right) + \left(\frac{1}{\beta}\right) \ln\left(t\right) \tag{7}$$

where α is the initial sorption rate (mg g^{-1} h^{-1}), and β (g mg^{-1}) is the desorption constant related to the extent of surface coverage and activation energy.

3. Results and discussion

3.1. Adsorbents characterization

3.1.1. SEM/SEM-EDX

The results obtained from the SEM for the adsorbents OP-TiO$_2$ and DS-TiO$_2$ after they were modified with TiO$_2$ NPs (Fig. 1-B and Fig. 1-D, respectively) indicated the presence of aggregates on the surface of the particles while in the unmodified materials (Fig. 1-A and Fig. 1-C), the images exhibited a smooth surface.

The EDS analysis revealed that the AC-OP and AC-DS (Fig. 2-A and Fig. 2-C) have similar chemical composition, with carbon the most abundant. The presence of TiO$_2$ was confirmed by the EDS for both adsorbents as shown in Fig. 2-B and Fig. 2-D.

3.1.2. XRD analysis

Fig. 3-A and Fig. 3-B shows the XRD patterns for the activated carbon from orange peels and date seeds after modification with TiO$_2$ NPs. In both adsorbents, $2\Theta = 25°$ validated the activated carbon existence [39]. The broadening diffusion peaks are depicted at small angles (<20°), which reveals that the activated carbon structure is amorphous with a heterogeneous surface [40]. The sharp peak at 30° confirmed that quartz was formed (SiO$_2$). The peaks at 25°, 36–38°, 48°, 52°, 54°, 62°, 69° and 75° indicate the presence and attachment of TiO$_2$ to activated carbon. All these diffractions peaks are well in accordance with typical pattern of anatase according to standard JCPDS card no. 89–492 [41].

3.1.3. Fourier transformed infrared radiation (FTIR)

The FTIR analysis in Fig. 4 represents the wavelength of modified activated date seed and orange peels by performing Fourier Transformed Infrared characterization technique for OP-TiO$_2$ and DS-TiO$_2$. The main peaks observed in the plots are explained in
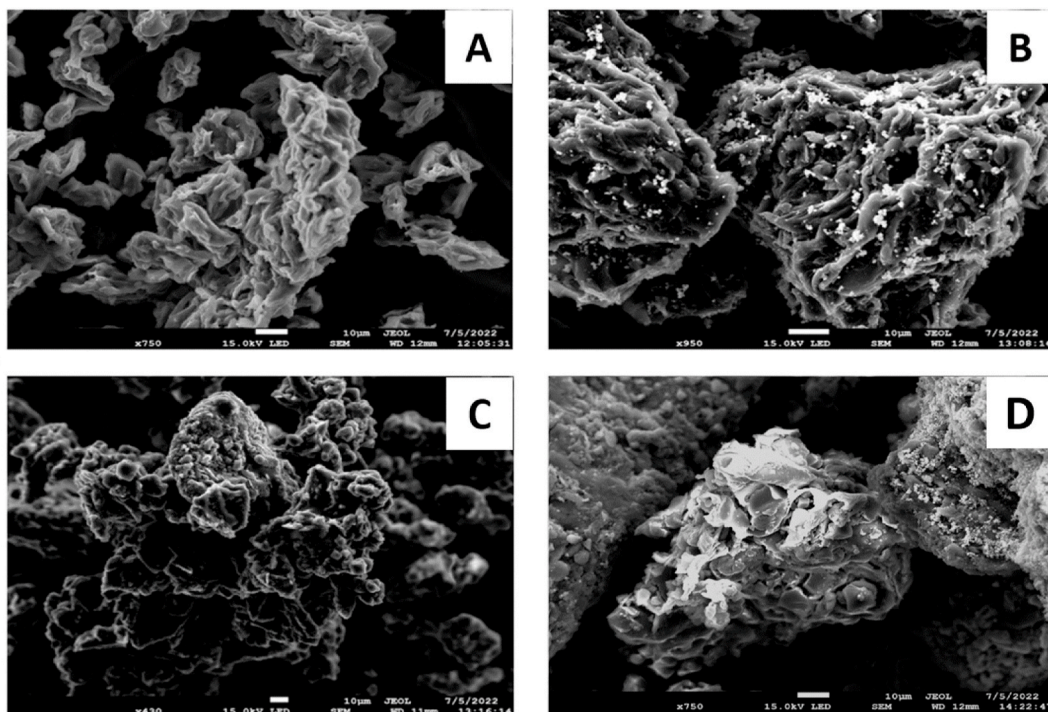

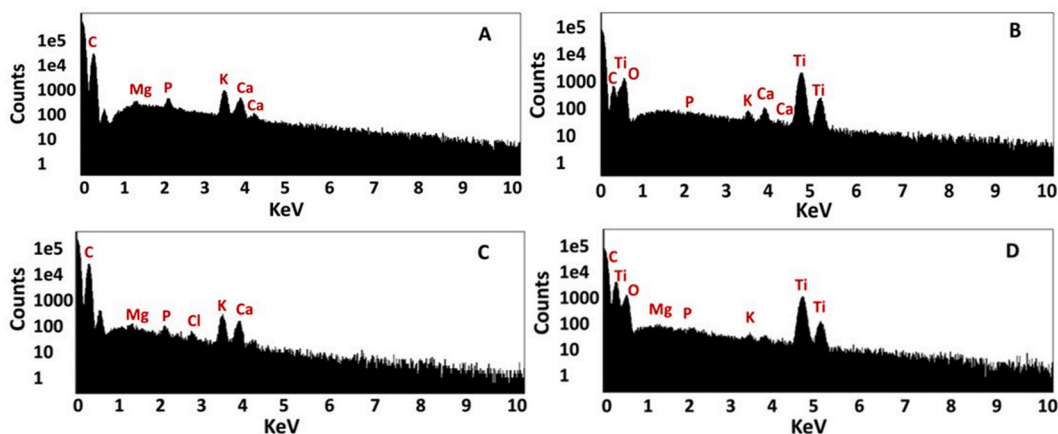**Fig. 1.** SEM image of (A) AC-OP, (B) OP-TiO$_2$, (C) AC-DS and D) DS-TiO$_2$.

Fig. 2. EDS graphs of (A) AC-OP, (B) OP-TiO$_2$, (C) AC-DS, and (D) DS-TiO$_2$.
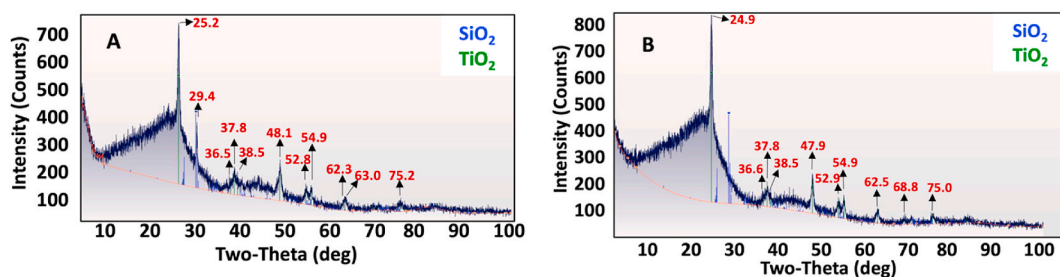

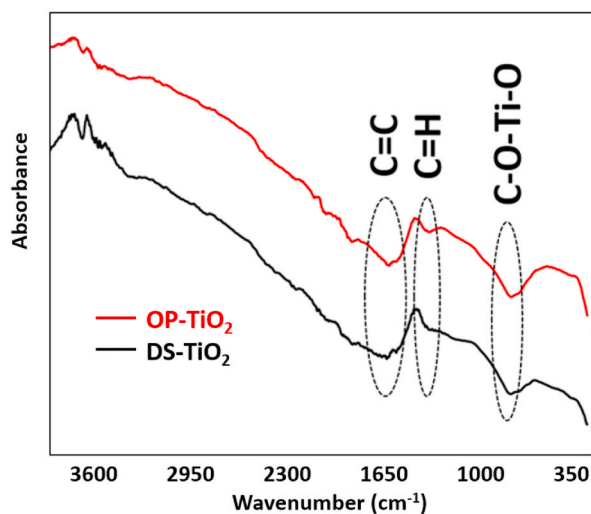**Fig. 3.** XRD patterns of (A) OP-TiO$_2$ and (B) DS-TiO$_2$.

Fig. 4. FTIR spectra of OP-TiO$_2$ and DS-TiO$_2$.

Table 3. According to the literature, the peaks around 800 cm^{-1} have been attributed to the Ti–O stretching bands and *C*–*O*–Ti–O bonding which indicated the attachment of titanium dioxide nanoparticles to activated carbon [39]. An –OH bending of alcoholic or carboxylic groups, or *C*–H bending vibrations, causes the peak to appear about 1473 cm^{-1} for OP-TiO$_2$ and 1480 cm^{-1} for DS-TiO$_2$ [42]. C=O bonds of the carboxyl groups were created and confirmed by peaks around peaks 1725 cm^{-1}. An aromatic ring vibration at the C=C stretching peak was found at 1660 and 1664 cm^{-1} for OP-TiO$_2$ and DS-TiO$_2$, respectively [39,43,44].

Table 3
FTIR spectra of OP-TiO$_2$ an DS-TiO$_2$.

Group	FTIR peak of	
	OP-TiO$_2$ (cm^{-1})	DS-TiO$_2$ (cm^{-1})
C–O–Ti–O bonding	850	772
C–H bending vibrations or O–H bending	1473	1480
C$=$C stretching in aromatic ring vibration or alkene	1660	1664
C$=$O stretching	1725	1725

3.1.4. Brunauer-Emmett-Teller (BET) theory

The surface area of the adsorbents was measured using the Brunauer-Emmett-Teller (BET) technique. As shown in Table 4, when the surface of activated carbon derived from orange peels and date seeds were modified by TiO$_2$, the surface area of the orange peel-based adsorbent was increased by approximately 150 %, while the date seed-based adsorbent experienced an increase of about 60 % compared to their respective original values. This increase in surface area can be attributed to the deposition of TiO$_2$ nanoparticles onto the surface of the activated carbon, leading to the creation of additional active sites and surface roughness. It is worth noting that the initial surface area of the date seed-based adsorbent is higher compared to that of the orange peel-based adsorbent which can be attributed to the structural and compositional differences between the two materials. However, the addition of TiO$_2$ resulted in a greater increase in the surface area of the orange peel-based adsorbent. This difference in surface area enhancement can be explained by the specific interactions between TiO$_2$ nanoparticles and the activated carbon matrix, which may vary between orange peels and date seeds, influencing the extent of surface area expansion. The presence of different functional groups and surface characteristics in each material might play a role in influencing the adsorption and deposition of TiO$_2$ nanoparticles. The results of BET analysis highlight the significance of modifying adsorbents to improve their performance in pollution removal applications.

3.2. Statistical analysis

The investigation on the impacts of four factors on the removal of Cu (%) was carried out through a total of 21 runs. Table 5 displays the results of the CCD matrix, demonstrating the removal efficiency (%) of Cu using OP-TiO$_2$ and DS-TiO$_2$.

According to the value of the coefficient of determination in Table 6 (R^2 = 0.91 and R^2 = 0.99), the regressions generated strong coefficient of determination showing each regression's validity, and a strong correlation between the actual and expected values [45]. In addition, the experiments' accuracy and dependability are further indicated by the relatively low coefficient of variation.

The analysis of variance (ANOVA; Table 7) was used to assess the statistical significance of the quadratic model. The F-values and p-values (Table 6), were used to assess each coefficient's significance. The greater the magnitude of the F-values and the smaller the p-values, the more significant the corresponding coefficients [46,47]. For both adsorbents, the model's terms are significant. Moreover, the lack-of-fit p-values greater than 0.05 are insignificant meaning that the proposed models in both cases managed to adequately describe the relation between the experimental variables and the adsorption efficiency [48,49]. According to Table 7, the linear effect of solution pH (A), initial ion concentration (B), and adsorbent dosage (C) was significant (p < 0.0001) and the contact time (D) linear effect was moderately significant (p = 0.1280) for DS-TiO$_2$; while for OP-TiO$_2$ the linear adsorbent dosage, and solution pH was significant (p < 0.0001) and the contact time and initial concentration linear effect was moderately significant. For DS-TiO$_2$, the effects of squared terms of B^2, A^2 and the interaction between AB, AC, and AD were significant; the effect of interaction between BD was slightly significant; however, the effects of interaction between other terms were not statistically significant. For OP-TiO$_2$, the effects of squared terms of C^2, A^2 and the interaction between BC was significant and for B^2 was slightly significant.

The level of Cu ion removal was determined by the regression equation, which was a function of the initial Cu ion concentration, pH, adsorbent dosage, and contact time. Cu ion removal (Y) and the variables' empirical relationship based on reduced polynomial equations are given in Table 8. The value of each factor to achieve the maximum adsorption efficiency is reported in Table 9. Eqs. (8) and (9) give the relationship between the examined process variables and copper removal efficiency for the developed adsorbents.

$$Cu\ removal\ (\%)\ by\ OP-TiO_2 = 89.47 + 2.91A - 1.25B + 8.49C + 3.19D + 5.02BC - 4.17A^2 + 2.81B^2 - 4.12C^2 \tag{8}$$

$$Cu\ removal\ (\%)\ by\ DS-TiO_2 = 31.57 + 25.34A - 36.29B + 6.55C + 1.03D - 10.06AB \\ + 4.37AC - 21.38AD + 1.67BD + 9.20A^2 - 3.62B^2 \tag{9}$$

Graphical methods were utilized to validate the CCD model by comparing the distribution of standardized residuals versus run plot

Table 4
Adsorbents results from BET analysis.

Samples	BET Surface area (m^2 g^{-1})
AC-OP	2.40
OP-TiO$_2$	6.06
AC-DS	51.10
DS-TiO$_2$	81.37

Table 5
The four-factors CCD matrix and experimental results for Cu removal.

Run	pH	Initial concentration (mg L^{-1})	Adsorbent dose (g L^{-1})	Contact time (h)	Removal efficiency (%)[a]	
					OP-TiO$_2$	DS-TiO$_2$
1	4	35	4.2	3	93.77 ± 2.48	30.80 ± 2.15
2	1	35	4.2	3	54.26 ± 2.15	14.40 ± 2.07
3	4	35	8	3	97.46 ± 2.75	42.34 ± 2.08
4	5.8	20	2	4.8	99.90 ± 7.85	77.00 ± 3.04
5	2.2	50	2	4.8	57.60 ± 2.3	6.68 ± 0.34
6	4	35	0.5	3	55.97 ± 4.53	19.94 ± 2.72
7	5.8	20	6.4	4.8	99.90 ± 2.28	97.40 ± 2.64
8	5.8	50	2	1.25	88.48 ± 4.76	22.84 ± 1.50
9	4	10	4.2	3	99.80 ± 2.86	82.40 ± 2.10
10	4	35	4.2	6	92.74 ± 2.50	34.40 ± 2.80
11	5.8	50	6.4	1.25	99.56 ± 2.12	46.08 ± 2.14
12	4	35	4.2	0.04	76.97 ± 2.13	30.97 ± 1.05
13	2.2	20	6.4	1.25	72.10 ± 2.06	19.10 ± 1.04
14	4	60	4.2	3	93.35 ± 4.12	31.88 ± 1.41
15	4	35	4.2	3	94.54 ± 5.73	15.90 ± 1.60
16	2.2	20	2	1.25	69.65 ± 0.89	28.85 ± 1.11
17	4	35	4.2	3	88.66 ± 2.31	12.20 ± 0.89
18	2.2	50	6.4	4.8	89.48 ± 3.24	32.06 ± 2.82
19	4	35	4.2	3	94.00 ± 2.43	33.66 ± 1.56
20	4	35	4.2	3	86.00 ± 2.75	99.94 ± 3.33
21	7	35	4.2	3	99.88 ± 5.09	30.80 ± 1.98

[a] Values are expressed as mean ± standard deviation of triplicate experiments.

Table 6
Fit statistics of response surface methodology model.

Adsorbent	Std. Dev.	Mean	C V %	R^2
OP-TiO$_2$	5.91	85.91	6.88	0.91
DS-TiO$_2$	1.46	38.94	3.74	0.99

Table 7
ANOVA for reduced quadratic modeling of Cu removal.

	Reduced Quadratic model (DS-TiO$_2$)					Reduced Quadratic model (OP–TiO$_2$)				
Source	Sum of Squares	df	Mean Square	F-value	p-value	Sum of Squares	df	Mean Square	F-value	p-value
Model	14799.32	10	1479.93	697.78	<0.0001	4246.09	8	530.76	15.21	<0.0001
A- pH	3563.15	1	3563.15	1680.00	<0.0001	2260.71	1	2260.71	64.80	<0.0001
B- initial concentration	1464.82	1	1464.82	690.65	<0.0001	21.45	1	21.45	0.61	0.4482
C- adsorbent dose	593.23	1	593.23	279.71	<0.0001	995.50	1	995.50	28.53	0.0002
D- contact time	5.96	1	5.96	2.81	0.1280	138.93	1	138.93	3.98	0.0692
AB	340.34	1	340.34	160.47	<0.0001					
AC	152.43	1	152.43	71.87	<0.0001					
AD	440.94	1	440.94	207.90	<0.0001					
BC						205.13	1	205.13	5.88	0.0320
BD	9.26	1	9.26	4.37	0.0662					
A^2	1068.21	1	1068.21	503.66	<0.0001	253.06	1	253.06	7.25	0.0196
B^2	57.67	1	57.67	27.19	0.0006	118.95	1	118.95	3.41	0.0896
C^2						266.57	1	266.57	7.64	0.0171
Residual	19.09	9	2.12			418.67	12	34.89		
Lack of Fit	6.51	5	1.30	0.41	0.8200	359.72	8	44.97	3.05	0.1481
Pure Error	12.58	4	3.14			58.94	4	14.74		
Cor Total	14818.41	19				4664.75	20			

Note: underlined p-values are not significant.

and the correlation between experimental and model-predicted values for Cu adsorption [27,50]. Fig. 5-A and Fig. 5-B display the actual and predicted removal efficiency values. The linear regression fit indicates that predicted values are in good agreement with the actual values. Fig. 5-C and Fig. 5-D illustrate scatter plots of residuals against the order of experimental runs, showing a uniform distribution of points without any discernible pattern or unusual structure which indicates that the model is appropriate and fits the data adequately.

Table 8
Coefficients in terms of coded factors.

Factor	Coefficient Estimate	
	OP-TiO$_2$	DS-TiO$_2$
Intercept	89.47	31.57
A-pH	+12.91	+25.34
B-initial concentration	−1.25	−36.29
C-adsorbent dose	+8.49	+6.55
D-contact time	+3.19	+1.03
AB	0	−10.06
AC	0	+4.37
AD	0	−21.38
BC	+5.02	0
BD	0	+1.67
CD	0	0
A^2	−4.17	+9.20
B^2	+2.81	−3.62
C^2	−4.12	0
D^2	0	0

Table 9
Optimal solutions for highest Cu removal efficiency.

Adsorbent	pH	Initial concentration (mg L^{-1})	Adsorbent dose (g L^{-1})	Contact time (h)	Desirability
OP-TiO$_2$	5.0	24.6	4.9	3.6	1.0
DS-TiO$_2$	6.4	21.2	5.0	3.0	1.0

The model's three-dimensional plots for Cu removal (percentage) as a function of pH-initial concentration and initial concentration-adsorbent dose for OP-TiO$_2$ and pH-adsorbent dose and pH-contact time for DS-TiO$_2$ is shown in Fig. 6. Fig. 6-A clearly demonstrates a substantial increase in Cu removal (%) with an increase in the adsorbent dose from 2 to 5.8 g L^{-1} and a decrease in the initial concentration from 50 to 20 mg L^{-1}, while maintaining the other factors constant (pH = 5 and contact time = 3.6 h). The plot (Fig. 6-B) illustrates that the removal of Cu (%) increased significantly as the solution pH increased from 2.2 to 6.4 and the initial concentration decreased from 50 to 20 mg L^{-1}, while the other factors were kept constant (adsorbent dose = 5 g L^{-1}, and contact time = 3 h). The pairwise interaction of pH and DS-TiO$_2$ dose, as depicted in Fig. 6-D, confirms that the removal efficiency slightly increased with the simultaneous increase of pH and contact time. Meanwhile, the other fixed parameters are initial concentration (20 mg L^{-1}) and adsorbent dose (5 g L^{-1}). It is evident from Fig. 6-C that the removal efficiency of Cu increased with an increase in the adsorbent dose from 2 to 6.4 g L^{-1}. This observation can be attributed to the higher number of active adsorption sites available at higher adsorbent doses. The highest Cu adsorption efficiency and adsorption capacity were 99.90 % and 13.34 mg g^{-1} for OP-TiO$_2$ and 97.40 % and 13.96 mg g^{-1} for DS-TiO$_2$. The performance of modified activated carbons for the adsorption of heavy metals is promising, attaining adsorption efficiency of >80 %, according to previous research [14,16,17,19,21,22]. The Comparison of the results of similar Cu adsorption studies using different adsorbents in Table 10 revealed that the removal efficiency of the OP-TiO$_2$ and DS-TiO$_2$ exhibited Cu removal efficiency and adsorbent capacity of developed adsorbents in this study is comparable to other adsorbents. Immobilized fungi residues were less effective, with a removal rate of only 73.11 % at a low concentration of 10 mg L^{-1} [51]. In terms of adsorbent dosage, the developed adsorbents in this study required a dosage of 5 g L^{-1} to achieve high removal rates, while peanut hull, and treated laterite required a much higher dosage of 20 g L^{-1}. However, compared to around 20 mg L^{-1} for Cu(II) in OP-TiO$_2$ and DS-TiO$_2$, the initial concentration for these experiments were also much higher at 150 mg L^{-1} and 200 mg L^{-1}, respectively [52,53]. On the other hand, some of the other adsorbents such as Luffa Actangula Carbon require a lower adsorbent dose of 1 g L^{-1} [54]. While most of the adsorbents required a shorter contact time of around 1–2 h [51–56], compared to this study, date seed biochar achieved a high removal rate of 96.96 % overnight [23]. The optimum pH for OP-TiO$_2$ and DS-TiO$_2$ was found to be 5, and 6.4, respectively, which is similar to other adsorbents ranging 4–6 [23,51–56]. It is important to note, however, that the effectiveness of an adsorbent in removing Cu(II) ions can be affected by a variety of factors, including the surface area and porosity of the adsorbent, chemical composition of the adsorbent, and experimental conditions used [57]. Additionally, other experimental conditions used such as temperature and agitation speed could also impact the adsorption efficiency of the adsorbents.

3.2.1. Effect of pH

The optimum pH for OP-TiO$_2$ and DS-TiO$_2$ was 5, and 6.4. Fig. 6-B shows the mutual effect of pH and initial concentration for OP-TiO$_2$ and pH and adsorbent dose (Fig. 6-C), pH and contact time (Fig. 6-D) for DS-TiO$_2$.

In the range of the experiment, increasing the pH increased the removal efficiency for both adsorbents. Similar trends were observed in many past studies; for instance, 20 mg EDTA-functionalized bamboo activated carbon (BAC) was added to 25 mL Pb(II) and Cu(II) solution and the findings showed that the equilibrium adsorption capacities for Pb(II) and Cu(II) increased for both ions
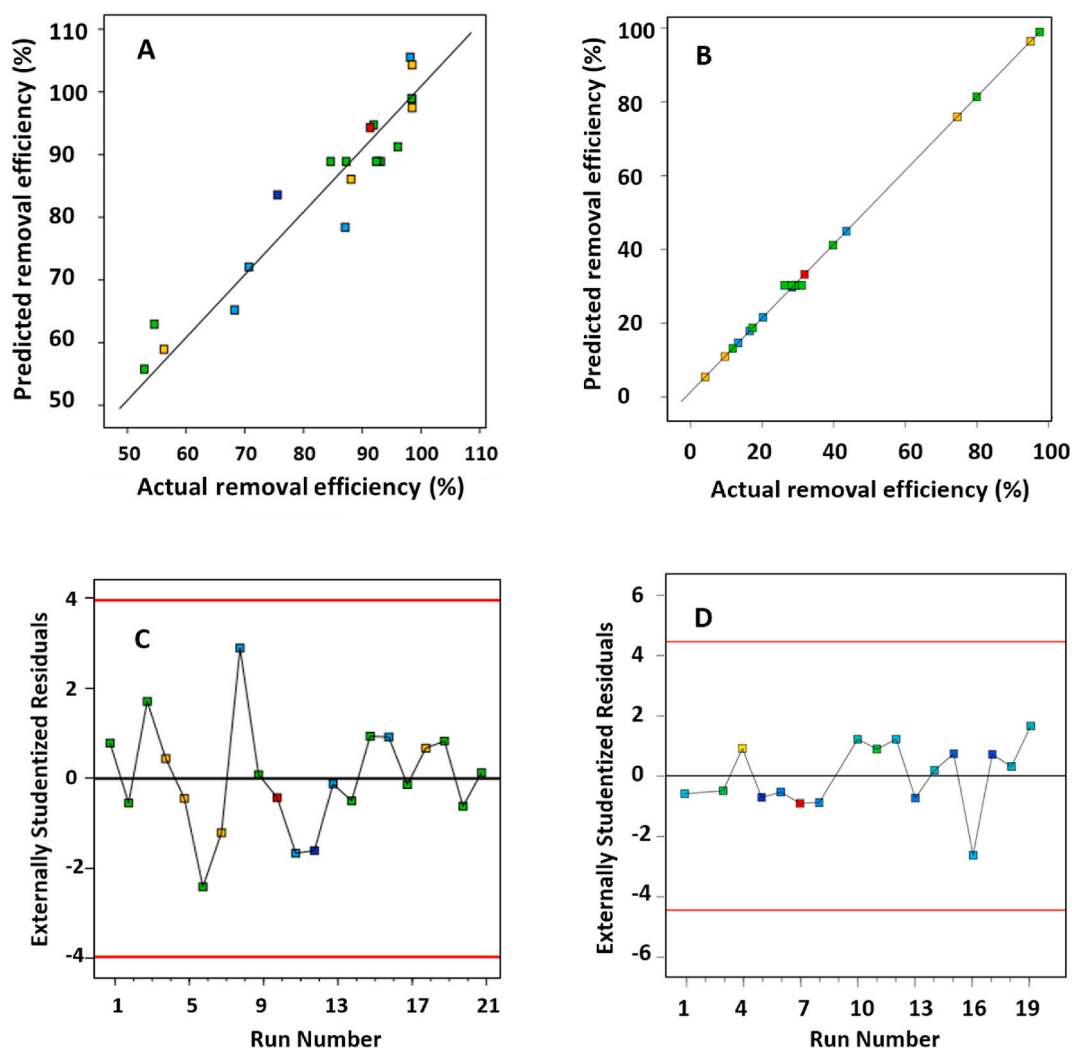
Fig. 5. Predicted vs actual values of removal efficiency for (A) orange peel (OP–TiO$_2$); (B) date seeds (DS-TiO$_2$); and residuals vs runs for (C) OP-TiO$_2$; and (D) DS-TiO$_2$. (For interpretation of the references to colour in this figure legend, the reader is referred to the Web version of this article.)

when pH increased from 2 to 6 [61]. In another case, as the solution pH increased, activated carbon and activated carbon impregnated with iron (III) were more effective at removing Cu(II) and for both adsorbents, it was found that Cu(II) was almost completely removed above pH 7 [62]. Other studies also revealed that the optimal pH range for adsorption performance is between 5 and 7. For example, Guo et al. (2011) and Amin et al. (2017) reported that the highest adsorption capacity of adsorbents occurs between pH 5 and 7 [18, 63].

3.2.2. Effect of adsorbent dose

The adsorption efficiency of OP-TiO$_2$ and DS-TiO$_2$ increased with increasing doses of adsorbent powder (Fig. 6-A and Fig. 6-C). Increasing the adsorbent mass indeed provides more active sites for heavy metal adsorption. Similarly, results of another study showed that the adsorption of 5.30 mg L^{-1} Pb(II) and 4.00 mg L^{-1} Cu(II) ions increased with increases in mass of biosorbent (2–10 g) from wastewater using activated carbon from cassava peels [64]. Amin et al. (2017) stated that increasing the adsorbent dose from 0.1 to 2.0 g L^{-1} increased the removal efficiency of Cu(II) from 20 % to 99.99 % for orange peel while in the case of date palm the removal efficiency increased from 12 % to 96 % at the same adsorbent dose [18].

3.2.3. Effect of initial concentration

In terms of initial concentration, for OP-TiO$_2$ (Fig. 6-B) and DS-TiO$_2$, increasing Cu initial concentration was found to decrease the removal efficiency, and the models predicted the optimum initial concentration was around 20 mg L^{-1}. The available active sites on the adsorbent are easily occupied with metal ions at low initial concentrations. The effects of initial concentration on the Pb(II) and Cu (II) adsorption by EDTA-functionalized bamboo activated carbon were similar. The increased initial concentration of Pb(II) and Cu(II)
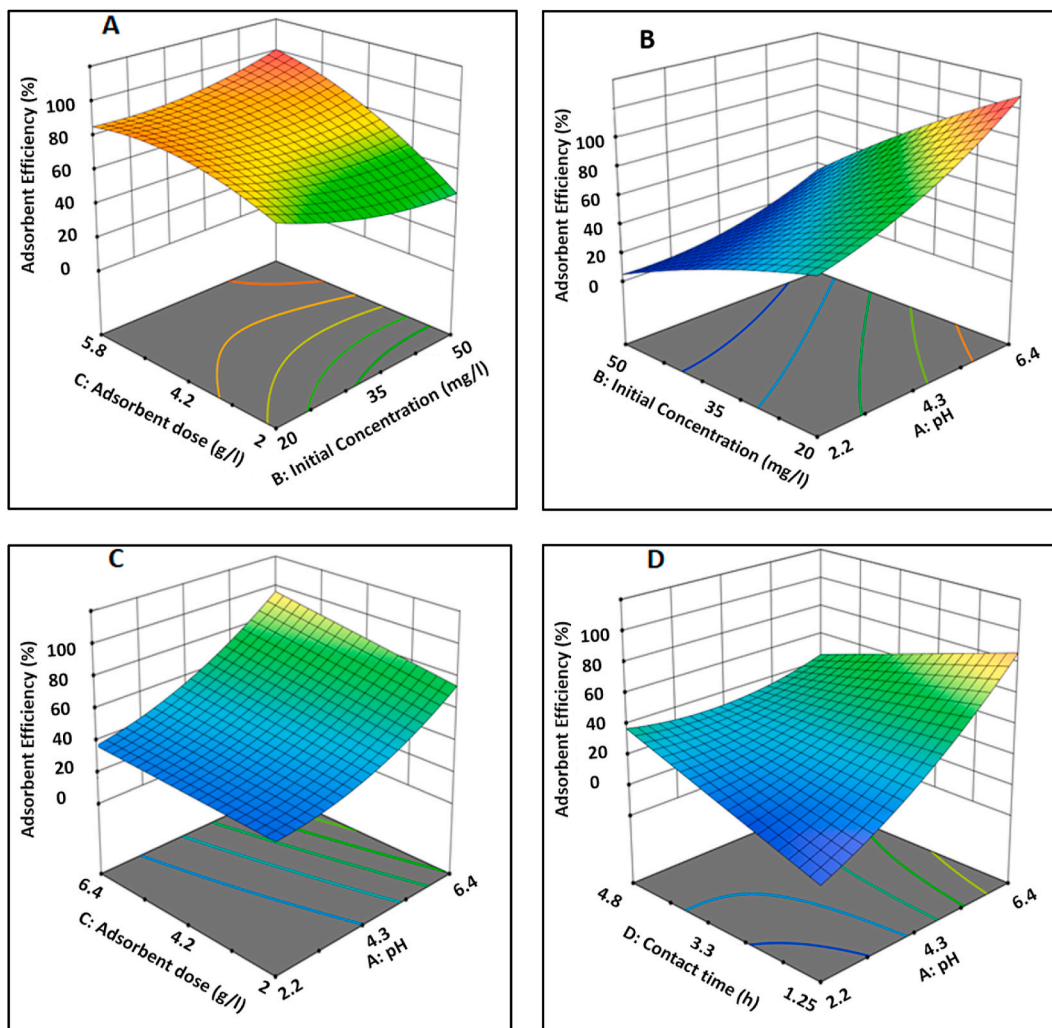
Fig. 6. Response surface maps of the effects of (A) initial concentration-adsorbent dose on the removal efficiency using OP-TiO$_2$ and (B) pH-Cu initial concentrations, (C) pH-adsorbent dose and (D) pH-contact time on the removal efficiency using DS-TiO$_2$. (Room temperature, rpm = 200).

led to improved equilibrium adsorption capacity before the active sites on the surface of the adsorbent were saturated while the equilibrium capacity stayed the same after that [61].

3.2.4. Effect of contact time

Increasing the contact time to more than 3 h did not significantly impact the Cu removal efficiency despite that the removal efficiency increased with increasing the contact time up to 3 h. Similarly in another study, at Cu(II) and Pb(II) concentrations of 100, 200, and 300 ppm, the adsorption capacities for Cu(II) and Pb(II) removal were studied as a function of the contact time and the adsorption capacity gradually increased with time. The maximum adsorption capabilities were attained after 180 min of contact time, and there was no further substantial increase [37].

3.3. Adsorption kinetic study

From the results, pseudo second-order model was best fitted to Cu adsorption for the case of OP- TiO$_2$ and DS-TiO$_2$. This observation implies that the adsorption process is governed by chemisorption. However, it is important to approach the interpretation of these models with caution, as complex matrices may involve a combination of chemisorption and physisorption mechanisms in the adsorption process [65,66]. Table 11 gives the kinetic parameters. Fig. 7 shows the kinetic plots for the pseudo first-order (Fig. 7-A and Fig. 7-B), pseudo second-order (Fig. 7-C and Fig. 7-D), intra-particle diffusion (Fig. 7-E and Fig. 7-F) and Elovich models (Fig. 7-G and Fig. 7-H), respectively. The R^2 values are 0.99 and 0.98 for OP-TiO$_2$ and DS-TiO$_2$, respectively, in the case of pseudo second-order. The Cu maximum equilibrium adsorption capacity (q$_e$) for OP-TiO$_2$ is 9.98 mg g^{-1}, while for DS-TiO$_2$ it is 9.95 mg g^{-1}. The results obtained from the fitting of the intraparticle diffusion model provide insights into the involvement of intraparticle diffusion in the adsorption

Table 10
Summary of adsorptive removal of copper by various adsorbents.

Adsorbent	Adsorbate	IC (mg L^{-1}) Unless indicated otherwise	Adsorbent dose (g L^{-1})	pH	Contact time (h)	Other Info	RE (%)/	AC (mg g^{-1})	Ref.
OP-TiO$_2$	Cu(II)	24.6	4.9	5.0	3.6	200 rpm 20 °C	99.9	13.34	This study
DS-TiO$_2$	Cu(II)	21.2	5.0	6.4	3.0	200 rpm 20 °C	97.4	13.96	This study
Date seeds biochar	Cu(II)	2.0	2.0		overnight	200 rpm	97.0		[23]
Carboxylated cellulose derivative (CTA)	Bicomponents: Cu^{2+}–Co^{2+}, Cu^{2+}–Ni^{2+}	0.8 mmol L^{-1}	0.2	5.5	1.0	25 °C 130 rpm		Cu^{2+}–Co^{2+} 0.99–0.24 mmol g^{-1} Cu^{2+}-Ni^{2+} 1.13–0.3 mmol g^{-1}	[55]
Peanut hull	Cu(II)	150.0	20.0	4.0	1.0	150 rpm 25 °C,		14.13	[52]
sugarcane bagasse (SG) acid modified sugarcane bagasse (ASG) base modified sugarcane bagasse (BSG) activated carbon (AC)	Cu(II)	10.0	5.0	5.0	1.0	150 rpm, 25 °C	SG: 88.9 ASG: 96.9 BSG: 94.8 AC: 98.5	4.84 5.35 2.06 5.62	[58]
Luffa Actangula Carbon	Cu(II)	50.0	1.0	6.0	2.0	30 °C		12.50	[54]
groundnut seed cake power, sesame seed cake powder, coconut cake powders	Cu(II)	10.0	15.0 20.0 20.0	5.0	0.5	40 °C		4.24	[59]
Immobilized fungi residues (*F. velutipes*)	Cu(II)	10.0	20.0	6.0	2.0	25 °C 150 rpm	73.1	8.13	[51]
Uncaria gambir	Cu(II)	10.0	1.2	5.0	1.5	60 °C 150 rpm		9.95	[60]

IC = initial concentration; RE = Removal efficiency; AC = Adsorption capacity; OP-TiO$_2$ = Activated carbon from orange peels modified by TiO$_2$; DS-TiO$_2$ = Activated carbon from date seeds modified by TiO$_2$.

Table 11
Kinetic parameters of four adsorptionkinetic models.

Model	Parameter	OP-TiO$_2$	DS-TiO$_2$
Pseudo first-order	k$_1$ (min^{-1})	-2.94×10^{-5}	-3.33×10^{-5}
	q$_e$ (mg g^{-1})	5.05	6.58
	R^2	0.71	0.88
Pseudo second-order	k$_2$ (g mg^{-1} min^{-1})	0.01	7.07×10^{-5}
	q$_e$ (mg g^{-1})	8.37	8.43
	R^2	0.99	0.98
Intraparticle diffusion	k_i (mg g^{-1} h$^{-0.5}$)	0.25	0.35
	C	4.72	2.96
	R^2	0.94	0.95
Elovich	α (mg g^{-1} h^{-1})	0.82	1.12
	β (g mg^{-1})	35.09	2.93
	R^2	0.92	0.91

process of Cu(II) onto the modified activated carbon adsorbents. If the adsorption process is solely controlled by intraparticle diffusion, the plot should yield a linear relationship that passes through the origin [67]. However, in reality, the plot often exhibits multiple linear segments, indicating the involvement of other factors. In this study, the fitting of the intraparticle diffusion model to the experimental data revealed that the plot of q_t against $t^{0.5}$ did not yield a single linear relationship but showed distinct linear segments. This suggests that the adsorption process of Cu(II) onto the modified activated carbon adsorbents involves multiple steps. The initial
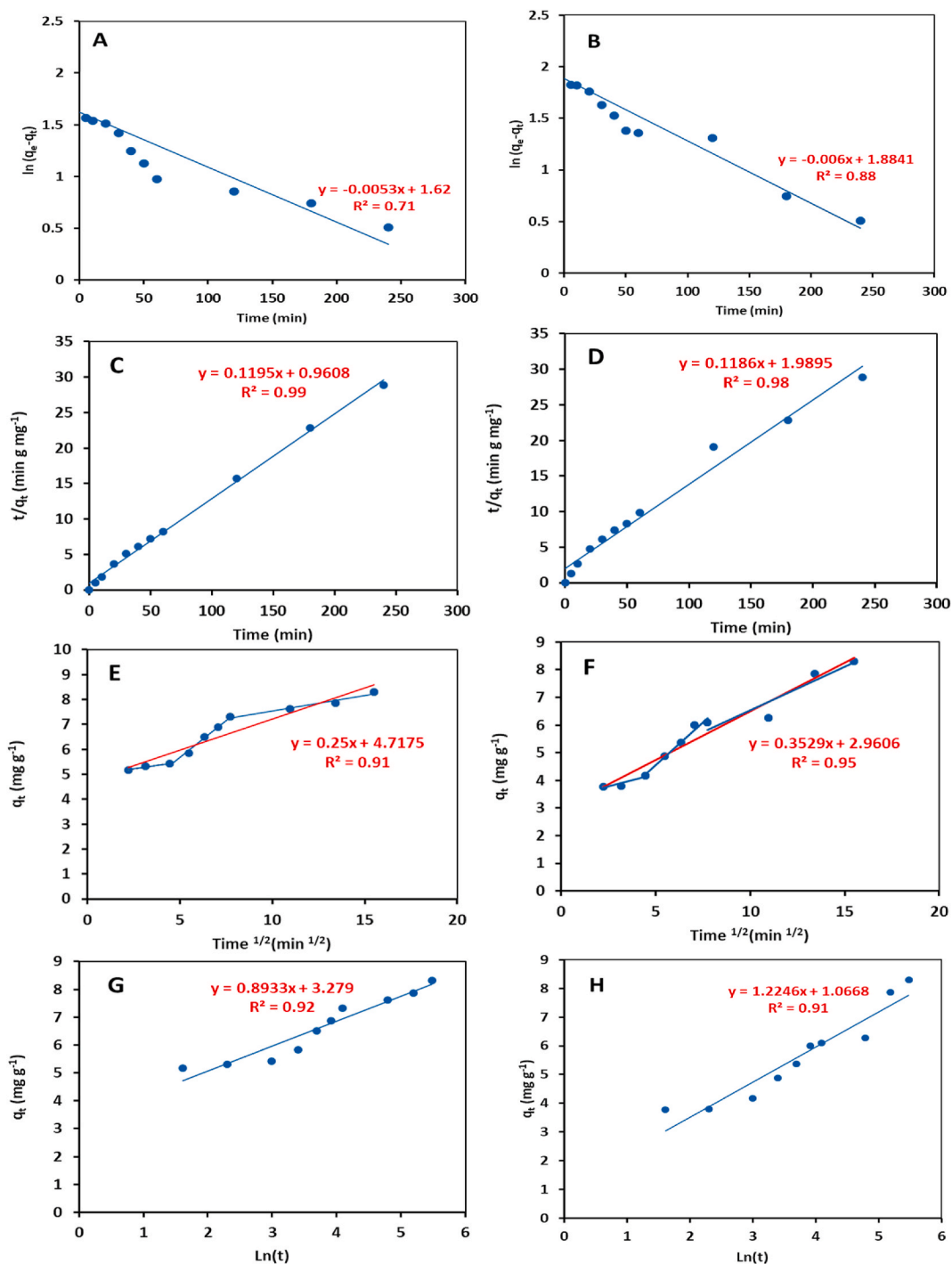
Fig. 7. Copper adsorption kinetic studies (A) Pseudo first-order-OP-TiO$_2$, (B) Pseudo first-order-DS-TiO$_2$ (C) Pseudo second order-OP-TiO$_2$, (D) Pseudo second-order-DS-TiO$_2$, (E) Intra-particle diffusion-OP-TiO$_2$, (F) Intra-particle diffusion-DS-TiO$_2$ (G) Elovich model-OP-TiO$_2$ and (H) Elovich model -DS-TiO$_2$. (Room temperature, rpm = 200, pH = 5 (OP–TiO$_2$), 5.4, initial concentration = 24.6 mg L^{-1} (OP–TiO$_2$), 21.2 mg L^{-1} (DS-TiO$_2$), Adsorbent dose = 4.9 g L^{-1} (OP–TiO$_2$), and 5 g L^{-1} (DS-TiO$_2$)).

steep section of the line indicates film diffusion, followed by another section where diffusion becomes the rate-controlling factor. The final part represents the equilibrium stage, where intraparticle diffusion slows down due to the low concentration of the remaining substance in the solution [68,69]. The adsorption rates for different stages were observed to exhibit the following order: the second stage > the third stage > the first stage for both adsorbents. Hence, the initial step (film diffusion) governs the overall rate of

adsorption. It is important to notice that the intercept (C) in the intraparticle diffusion model represents the thickness of the boundary layer. A higher intercept value indicates a thicker boundary layer, which could potentially hinder the diffusion process and affect the overall adsorption rate [70].

3.4. Strengths, limitations, and recommendations

One of the major strengths of this study is utilizing waste materials (orange peels and date seeds) as precursors for the modified activated carbon. This study adds value to waste and promotes sustainable practices by repurposing these abundant and easily accessible materials. Another notable strength of this study is using the Response Surface Methodology (RSM) and Central Composite Design (CCD) for optimization. Applying RSM allows for a systematic and efficient exploration of the process variables, and identifies the optimal conditions for copper removal. Additionally, the results from the batch Cu^{2+} adsorption experiments demonstrate the synthesized adsorbents effectiveness in removing copper from water.

A limitation of this study is the use of synthetic water instead of real water samples. While synthetic water provides controlled conditions for experimentation, it may not fully represent the complex composition of real-world water sources, which can contain various ions and contaminants. Future studies should consider investigating the adsorption performance of the developed adsorbents using real water samples to assess its efficacy in practical applications. Furthermore, it is recommended to conduct continuous flow studies to evaluate the performance of the OP-TiO$_2$ and DS-TiO$_2$ under continuous operation. Continuous flow experiments can provide insights into the long-term stability and efficiency of the adsorbent in real-world scenarios. Furthermore, investigating the adsorbent regeneration feasibility and assessing its stability and reusability would contribute to the development of cost-effective and sustainable water treatment processes. Another important thing to consider is recovering the adsorbents after water treatment, which presents a challenge for their reusability. It is important to address the potential release of TiO$_2$ nanoparticles into the environment and investigate their behavior and long-term effects thoroughly. It is recommended to focus on developing safe disposal methods and exploring the potential for recycling or reusing the spent adsorbents. These efforts will contribute to the overall sustainability and minimize any potential environmental impact.

4. Conclusions

A TiO$_2$ nanoparticles-modified activated carbon has been successfully developed from orange peels (OP) and date seeds (DS). Modifying the activated carbon with TiO$_2$ increased the surface area of both adsorbents. The developed adsorbent (OP–TiO$_2$ and DS-TiO$_2$) can significantly remove Cu ions from aquatic solutions with a removal efficiency of 99.90 % and 97.40 %, respectively, after about 3 h. The highest adsorption efficiency for OP-TiO$_2$ was predicted at pH 5.0, adsorbent dose of 4.9 g L^{-1}, contact time 3.6 h, and initial Cu concentration of 24.6 mg L^{-1}, based on the RSM-CCD. A similar optimum condition has been found for DS-TiO$_2$ at pH 6.4, adsorbent dose of 5.0g L^{-1}, contact time 3.0 h, and initial Cu concentration of 21.2 mg L^{-1}. The highest adsorption capacity was 13.34 mg g^{-1} for OP-TiO$_2$ and 13.96 mg g^{-1} for DS-TiO$_2$. The experimental data were fitted to several kinetic models, and the results revealed that the Cu sorption on OP-TiO$_2$ (R^2 = 0.99, k$_2$ = 0.01 g mg^{-1} min^{-1}, and q$_e$ = 8.37 mg g^{-1}) and DS-TiO$_2$ (R^2 = 0.98, k$_2$ = 7.07 × 10^{-5} g mg^{-1} min^{-1}, and q$_e$ = 8.43 mg g^{-1}) could be better described by the pseudo second-order kinetic.

The exceptional heavy metal removal capability of these renewable and affordable adsorbents from locally accessible sources was proven. More research is required to replace commercial activated carbon with environmentally friendly adsorbents such as OP-TiO$_2$ and DS-TiO$_2$ to be successfully used in water and wastewater treatment plants.

Data availability statement

The data are provided in the paper.

Additional information

No additional information is available for this paper.

CRediT authorship contribution statement

Roya Sadat Neisan: Investigation, Writing – original draft. **Noori M.Cata Saady:** Funding acquisition, Investigation, Methodology, Project administration, Resources, Supervision, Validation, Writing – original draft, Writing – review & editing. **Carlos Bazan:** Project administration, Supervision, Writing – review & editing. **Sohrab Zendehboudi:** Resources, Writing – review & editing. **Talib M. Albayati:** Writing – review & editing.

Declaration of competing interest

The authors declare that they have no known competing financial interests or personal relationships that could have appeared to influence the work reported in this paper.

Acknowledgements

References

[1] Z. Fu, S. Xi, The effects of heavy metals on human metabolism, Toxicol. Mech. Methods 30 (2020) 167–176.
[2] L. Joseph, B.-M. Jun, J.R. V Flora, C.M. Park, Y. Yoon, Removal of heavy metals from water sources in the developing world using low-cost materials: a review, Chemosphere 229 (2019) 142–159.
[3] Ł. Stala, J. Ulatowska, I. Polowczyk, Copper (II) ions removal from model galvanic wastewater by green one-pot synthesised amino-hypophosphite polyampholyte, J. Hazard Mater. 436 (2022), 129047.
[4] S.P. Lenka, W.A. Shaikh, G. Owens, L.P. Padhye, S. Chakraborty, T. Bhattacharya, Removal of copper from water and wastewater using dolochar, Water, Air, Soil Pollut. 232 (2021) 1–15.
[5] Y. Zhang, X. Yue, W. Xu, H. Zhang, F. Li, Amino modification of rice straw-derived biochar for enhancing its cadmium (II) ions adsorption from water, J. Hazard Mater. 379 (2019), 120783.
[6] S. Deng, R. Bai, J.P. Chen, Aminated polyacrylonitrile fibers for lead and copper removal, Langmuir 19 (2003) 5058–5064.
[7] A.M. Azzam, S.T. El-Wakeel, B.B. Mostafa, M.F. El-Shahat, Removal of Pb, Cd, Cu and Ni from aqueous solution using nano scale zero valent iron particles, J. Environ. Chem. Eng. 4 (2016) 2196–2206.
[8] J. Lin, Y. Zhan, Z. Zhu, Adsorption characteristics of copper (II) ions from aqueous solution onto humic acid-immobilized surfactant-modified zeolite, Colloids Surfaces A Physicochem. Eng. Asp. 384 (2011) 9–16.
[9] N. Asim, M.H. Amin, N.A. Samsudin, M. Badiei, H. Razali, M. Akhtaruzzaman, N. Amin, K. Sopian, Development of effective and sustainable adsorbent biomaterial from an agricultural waste material: Cu (II) removal, Mater. Chem. Phys. 249 (2020), 123128.
[10] A. Méndez, S. Barriga, J.M. Fidalgo, G. Gascó, Adsorbent materials from paper industry waste materials and their use in Cu (II) removal from water, J. Hazard Mater. 165 (2009) 736–743.
[11] M.F. Elkady, M.M. Hussein, H.M. Atiaa, Preparation of nano-activated carbon from carbon based material for copper decontamination from wastewater, Am. J. Appl. Chem. 3 (2015) 31–37.
[12] S. Hydari, H. Sharififard, M. Nabavinia, M. reza Parvizi, A comparative investigation on removal performances of commercial activated carbon, chitosan biosorbent and chitosan/activated carbon composite for cadmium, Chem. Eng. J. 193 (2012) 276–282.
[13] K.B. Tan, M. Vakili, B.A. Horri, P.E. Poh, A.Z. Abdullah, B. Salamatinia, Adsorption of dyes by nanomaterials: recent developments and adsorption mechanisms, Sep. Purif. Technol. 150 (2015) 229–242.
[14] M.L. Faisal, S.Z. Al-Najjar, Z.T. Al-Sharify, Modified orange peel as sorbent in removing of heavy metals from aqueous solution, J. Green Eng. 10 (2020) 10600–10615.
[15] F. Meng, B. Yang, B. Wang, S. Duan, Z. Chen, W. Ma, Novel dendrimerlike magnetic biosorbent based on modified orange peel waste: adsorption–reduction behavior of arsenic, ACS Sustain. Chem. Eng. 5 (2017) 9692–9700.
[16] S. Pavithra, G. Thandapani, S. Sugashini, P.N. Sudha, H.H. Alkhamis, A.F. Alrefaei, M.H. Almutairi, Batch adsorption studies on surface tailored chitosan/orange peel hydrogel composite for the removal of Cr (VI) and Cu (II) ions from synthetic wastewater, Chemosphere 271 (2021), 129415.
[17] K. Shehzad, C. Xie, J. He, X. Cai, W. Xu, J. Liu, Facile synthesis of novel calcined magnetic orange peel composites for efficient removal of arsenite through simultaneous oxidation and adsorption, J. Colloid Interface Sci. 511 (2018) 155–164.
[18] M.T. Amin, A.A. Alazba, M.N. Amin, Absorption behaviours of copper, lead, and arsenic in aqueous solution using date palm fibres and orange peel: kinetics and thermodynamics, Pol. J. Environ. Stud. 26 (2017).
[19] A. Elkhaleefa, I.H. Ali, E.I. Brima, A.B. Elhag, B. Karama, Efficient removal of Ni (II) from aqueous solution by date seeds powder biosorbent: adsorption kinetics, Isotherm. Thermodyn., Processes 8 (2020) 1001.
[20] K. Rambabu, F. Banat, G.S. Nirmala, S. Velu, P. Monash, G. Arthanareeswaran, Activated carbon from date seeds for chromium removal in aqueous solution, Desalination Water Treat. 156 (2019) 267–277.
[21] S.N.H. Azmi, M. Al-Balushi, F. Al-Siyabi, N. Al-Hinai, S. Khurshid, Adsorptive removal of Pb (II) ions from groundwater samples in Oman using carbonized Phoenix dactylifera seed (Date stone), J. King Saud Univ. 32 (2020) 2931–2938.
[22] T.M. Khan, I. Riaz, S. Hameed, B. Khan, Lemon juice and microwave assisted modification of date seed husk for arsenic biosorption, J. Innov. Sci. 5 (2019) 106–114.
[23] A.A.J. Mohamed, L.A. Vuai, M. Kombo, O.J. Chukwuma, Removal of selected metal ions using powder of seeds of Ajwaa dates from aqueous solution, J. Anal. Pharm Res. 8 (2019) 228–232.
[24] W. Gan, X. Shang, X.-H. Li, J. Zhang, X. Fu, Achieving high adsorption capacity and ultrafast removal of methylene blue and Pb2+ by graphene-like TiO2@ C, Colloids Surfaces A Physicochem. Eng. Asp. 561 (2019) 218–225.
[25] F. Vajedi, H. Dehghani, The characterization of TiO2-reduced graphene oxide nanocomposites and their performance in electrochemical determination for removing heavy metals ions of cadmium (II), lead (II) and copper (II), Mater. Sci. Eng. B 243 (2019) 189–198.
[26] M.A. Ajala, A.S. Abdulkareem, J.O. Tijani, A.S. Kovo, Adsorptive behaviour of rutile phased titania nanoparticles supported on acid-modified kaolinite clay for the removal of selected heavy metal ions from mining wastewater, Appl. Water Sci. 12 (2022) 19.
[27] A.S. Abdulhameed, N.N.M.F. Hum, S. Rangabhashiyam, A.H. Jawad, L.D. Wilson, Z.M. Yaseen, A.A. Al-Kahtani, Z.A. Alothman, Statistical modeling and mechanistic pathway for methylene blue dye removal by high surface area and mesoporous grass-based activated carbon using K2CO3 activator, J. Environ. Chem. Eng. 9 (2021), 105530.
[28] A.H. Jawad, M.A.M. Ishak, A.M. Farhan, K. Ismail, Response surface methodology approach for optimization of color removal and COD reduction of methylene blue using microwave-induced NaOH activated carbon from biomass waste, Water Treat. 62 (2017) 208–220.
[29] A.H. Jawad, M. Bardhan, M.A. Islam, M.A. Islam, S.S.A. Syed-Hassan, S.N. Surip, Z.A. Alothman, M.R. Khan, Insights into the modeling, characterization and adsorption performance of mesoporous activated carbon from corn cob residue via microwave-assisted H3PO4 activation, Surface. Interfac. 21 (2020), 100688.
[30] G.G. Bessegato, L.C. De Almeida, S.L.C. Ferreira, M.V.B. Zanoni, Experimental design as a tool for parameter optimization of photoelectrocatalytic degradation of a textile dye, J. Environ. Chem. Eng. 7 (2019), 103264.
[31] C.Y. Chaware, M.U. Khobragade, RECENT ADVANCEMENT IN PROCESS OPTIMIZATION USING RSM FOR ADSORPTIVE REMOVAL OF DYES FROM AQUEOUS SOLUTIONS: A REVIEW, (n.d.)..
[32] M. Salari, M.R. Nikoo, A. Al-Mamun, G.R. Rakhshandehroo, M.G. Mooselu, Optimizing Fenton-like process, homogeneous at neutral pH for ciprofloxacin degradation: comparing RSM-CCD and ANN-GA, J. Environ. Manag. 317 (2022), 115469.

[33] D. Pantazis, S.G. Pease, P. Goodall, A. West, P. Conway, A design of experiments Cyber–Physical System for energy modelling and optimisation in end-milling machining, Robot. Comput. Integrated Manuf. 80 (2023), 102469.

[34] P. Ghahri, M. Jamiolahmady, M. Sohrabi, A thorough investigation of cleanup efficiency of hydraulic fractured wells using response surface methodology, in: SPE Eur. Form. Damage Conf. Exhib., SPE, 2011, SPE-144114.

[35] A.H. Jawad, A.S. Abdulhameed, L.D. Wilson, S.S.A. Syed-Hassan, Z.A. Alothman, M.R. Khan, High surface area and mesoporous activated carbon from KOH-activated dragon fruit peels for methylene blue dye adsorption: optimization and mechanism study, Chin. J. Chem. Eng. 32 (2021) 281–290.

[36] E. Vunain, D. Kenneth, T. Biswick, Synthesis and characterization of low-cost activated carbon prepared from Malawian baobab fruit shells by H3PO4 activation for removal of Cu (II) ions: equilibrium and kinetics studies, Appl. Water Sci. 7 (2017) 4301–4319.

[37] Z.A. Alothman, M.A. Habila, N.H. Al-Shalan, S.M. Alfadul, R. Ali, B. Alfarhan, Adsorptive removal of Cu (II) and Pb (II) onto mixed-waste activated carbon: kinetic, thermodynamic, and competitive studies and application to real wastewater samples, Arabian J. Geosci. 9 (2016) 1–9.

[38] S. Mishra, G. Achary, M. Das, Adsorption of Cu (II) by used aqua guard carbon (UAC), J. Chem. Pharmaceut. Res. 4 (2012) 1207–1216.

[39] C. Parvathiraja, S. Katheria, M.R. Siddiqui, S.M. Wabaidur, M.A. Islam, W.-C. Lai, Activated carbon-loaded titanium dioxide nanoparticles and their photocatalytic and antibacterial investigations, Catalysts 12 (2022) 834.

[40] F.E. Pujiono, T.A. Mulyati, M.N. Fizakia, Modification of activated carbon with titanium dioxide as a water treatment material, J. Publ. Health Afr. 10 (2019).

[41] F. Ahmed, C. Awada, S.A. Ansari, A. Aljaafari, A. Alshoaibi, Photocatalytic inactivation of Escherichia coli under UV light irradiation using large surface area anatase TiO2 quantum dots, R. Soc. Open Sci. 6 (2019), 191444.

[42] N. Taoufik, A. Elmchaouri, F. Anouar, S.A. Korili, A. Gil, Improvement of the adsorption properties of an activated carbon coated by titanium dioxide for the removal of emerging contaminants, J. Water Process Eng. 31 (2019), 100876.

[43] H. Bamdad, A Theoretical and Experimental Study on Biochar as an Adsorbent for Removal of Acid Gases, CO₂ and H₂S), 2019.

[44] V.K. Gupta, A. Nayak, Cadmium removal and recovery from aqueous solutions by novel adsorbents prepared from orange peel and Fe2O3 nanoparticles, Chem. Eng. J. 180 (2012) 81–90.

[45] A.H. Jawad, I.A. Mohammed, A.S. Abdulhameed, Tuning of fly ash loading into chitosan-ethylene glycol diglycidyl ether composite for enhanced removal of reactive red 120 dye: optimization using the Box–Behnken design, J. Polym. Environ. 28 (2020) 2720–2733.

[46] S. Afshin, Y. Rashtbari, M. Vosough, A. Dargahi, M. Fazlzadeh, A. Behzad, M. Yousefi, Application of Box–Behnken design for optimizing parameters of hexavalent chromium removal from aqueous solutions using Fe3O4 loaded on activated carbon prepared from alga: kinetics and equilibrium study, J. Water Process Eng. 42 (2021), 102113.

[47] M.H. Dehghani, A.H. Hassani, R.R. Karri, B. Younesi, M. Shayeghi, M. Salari, A. Zarei, M. Yousefi, Z. Heidarinejad, Process optimization and enhancement of pesticide adsorption by porous adsorbents by regression analysis and parametric modelling, Sci. Rep. 11 (2021), 11719.

[48] M. Yousefi, M. Gholami, V. Oskoei, A.A. Mohammadi, M. Baziar, A. Esrafili, Comparison of LSSVM and RSM in simulating the removal of ciprofloxacin from aqueous solutions using magnetization of functionalized multi-walled carbon nanotubes: process optimization using GA and RSM techniques, J. Environ. Chem. Eng. 9 (2021), 105677.

[49] A. Reghioua, D. Barkat, A.H. Jawad, A.S. Abdulhameed, A.A. Al-Kahtani, Z.A. Alothman, Parametric optimization by Box–Behnken design for synthesis of magnetic chitosan-benzil/ZnO/Fe3O4 nanocomposite and textile dye removal, J. Environ. Chem. Eng. 9 (2021), 105166.

[50] R. Ghelich, M.R. Jahannama, H. Abdizadeh, F.S. Torknik, M.R. Vaezi, Central composite design (CCD)-Response surface methodology (RSM) of effective electrospinning parameters on PVP-B-Hf hybrid nanofibrous composites for synthesis of HfB2-based composite nanofibers, Composites, Part B 166 (2019) 527–541.

[51] X. Li, D. Zhang, F. Sheng, H. Qing, Adsorption characteristics of Copper (II), Zinc (II) and Mercury (II) by four kinds of immobilized fungi residues, Ecotoxicol. Environ. Saf. 147 (2018) 357–366.

[52] R.M. Ali, H.A. Hamad, M.M. Hussein, G.F. Malash, Potential of using green adsorbent of heavy metal removal from aqueous solutions: adsorption kinetics, isotherm, thermodynamic, mechanism and economic analysis, Ecol. Eng. 91 (2016) 317–332.

[53] K.S. Rani, B. Srinivas, K. GouruNaidu, K. V Ramesh, Removal of copper by adsorption on treated laterite, Mater. Today Proc. 5 (2018) 463–469.

[54] S.H. Siddiqui, The removal of Cu2+, Ni2+ and methylene blue (MB) from aqueous solution using Luffa Actangula carbon: kinetics, thermodynamic and isotherm and response methodology, Groundw. Sustain. Dev. 6 (2018) 141–149.

[55] F.S. Teodoro, O.F.H. Adarme, L.F. Gil, L.V.A. Gurgel, Synthesis and application of a new carboxylated cellulose derivative. Part II: removal of Co2+, Cu2+ and Ni2+ from bicomponent spiked aqueous solution, J. Colloid Interface Sci. 487 (2017) 266–280.

[56] X. Liu, Z.-Q. Chen, B. Han, C.-L. Su, Q. Han, W.-Z. Chen, Biosorption of copper ions from aqueous solution using rape straw powders: optimization, equilibrium and kinetic studies, Ecotoxicol. Environ. Saf. 150 (2018) 251–259.

[57] B. Qiu, X. Tao, H. Wang, W. Li, X. Ding, H. Chu, Biochar as a low-cost adsorbent for aqueous heavy metal removal: a review, J. Anal. Appl. Pyrolysis 155 (2021), 105081.

[58] M. Gupta, H. Gupta, D.S. Kharat, Adsorption of Cu (II) by low cost adsorbents and the cost analysis, Environ. Technol. Innov. 10 (2018) 91–101.

[59] G. Pavan Kumar, K.A. Malla, B. Yerra, K. Srinivasa Rao, Removal of Cu (II) using three low-cost adsorbents and prediction of adsorption using artificial neural networks, Appl. Water Sci. 9 (2019) 1–9.

[60] K.S. Tong, M.J. Kassim, A. Azraa, Adsorption of copper ion from its aqueous solution by a novel biosorbent Uncaria gambir: equilibrium, kinetics, and thermodynamic studies, Chem. Eng. J. 170 (2011) 145–153.

[61] D. Lv, Y. Liu, J. Zhou, K. Yang, Z. Lou, S.A. Baig, X. Xu, Application of EDTA-functionalized bamboo activated carbon (BAC) for Pb (II) and Cu (II) removal from aqueous solutions, Appl. Surf. Sci. 428 (2018) 648–658.

[62] J.-K. Yang, H.-J. Park, H.-D. Lee, S.-M. Lee, Removal of Cu (II) by activated carbon impregnated with iron (III), Colloids Surfaces A Physicochem. Eng. Asp. 337 (2009) 154–158.

[63] J. Fang, G. Qin, W. Wei, X. Zhao, Preparation and characterization of tubular supported ceramic microfiltration membranes from fly ash, Sep. Purif. Technol. 80 (2011) 585–591.

[64] H.I. Owamah, Biosorptive removal of Pb (II) and Cu (II) from wastewater using activated carbon from cassava peels, J. Mater. Cycles Waste Manag. 16 (2014) 347–358.

[65] I. Chopra, P.K. Singh, S.B. Singh, Kinetics and equilibrium studies for methylene blue removal from simulated wastewater effluents using agricultural waste, Parthenium hysterophorus L, Indian J. Chem. Technol. 27 (2020) 274–282.

[66] T.B. da Costa, T.L. da Silva, M.G.C. da Silva, M.G.A. Vieira, Efficient recovery of europium by biosorption and desorption using beads developed from sericin residues from silk yarns processing, sodium alginate and poly (ethylene glycol) diglycidyl ether, J. Environ. Chem. Eng. 11 (2023), 109222.

[67] Z. Wu, H. Zhong, X. Yuan, H. Wang, L. Wang, X. Chen, G. Zeng, Y. Wu, Adsorptive removal of methylene blue by rhamnolipid-functionalized graphene oxide from wastewater, Water Res. 67 (2014) 330–344.

[68] G.F. Malash, M.I. El-Khaiary, Piecewise linear regression: a statistical method for the analysis of experimental adsorption data by the intraparticle-diffusion models, Chem. Eng. J. 163 (2010) 256–263.

[69] M. Claros, J. Kuta, O. El-Dahshan, J. Michalička, Y.P. Jimenez, S. Vallejos, Hydrothermally synthesized MnO2 nanowires and their application in Lead (II) and Copper (II) batch adsorption, J. Mol. Liq. 325 (2021), 115203.

[70] Q. Du, J. Sun, Y. Li, X. Yang, X. Wang, Z. Wang, L. Xia, Highly enhanced adsorption of Congo red onto graphene oxide/chitosan fibers by wet-chemical etching off silica nanoparticles, Chem. Eng. J. 245 (2014) 99–106.